Hindawi
Geofluids
Volume 2019, Article ID 6315947, 12 pages
https://doi.org/10.1155/2019/6315947

Research Article

Relationship between Blocking Performance and Foam Texture in Porous Media

Zhuangzhuang Wang[1], **Zhaomin Li**[1], **Hailong Chen**[1], **Fei Wang**[2], **Dawei Hou**[1] and **Yajie Xu**[1]

[1]*College of Petroleum Engineering, China University of Petroleum (East China), Qingdao, 266580 Shandong, China*
[2]*Geo-Energy Research Institute, Faculty of Electromechanical Engineering, Qingdao University of Science and Technology, Qingdao, 266061 Shandong, China*

Correspondence should be addressed to Zhaomin Li; lizhm@upc.edu.cn

Received 21 August 2018; Revised 8 November 2018; Accepted 13 December 2018; Published 28 January 2019

Academic Editor: Zhenjiang You

Foam is widely used as a selective blocking agent through mobility control in oil field development. Its flow behavior in porous media has been investigated sufficiently, but few studies were carried out to understand the change of foam texture in flow. In this work, sandpack and micromodel experiments were conducted simultaneously to analyze foam flow behavior from the perspective of foam texture. Based on the measured flowing pressure and the observed foam image, the correlation between blocking pressure and foam texture was quantitatively investigated. The blocking pressure has a strong correlation with average diameter (-0.906) and variation coefficient (-0.78) and has a positive correlation with the filling ratio (0.84). These indicate that the blocking performance of foam is influenced by its texture closely. But path analysis shows only that the average diameter and variation coefficient have a significant direct effect on blocking pressure (-0.624 and -0.404). These show that the blocking capacity of foam is mainly influenced by the size and uniformity of bubbles. Tiny, dense, and homogeneous foam has a stronger blocking capacity. This study provides a deep insight of foam flow in porous media.

1. Introduction

Foam, as a gas-liquid dispersion system, is widely used in oilfield development with the characteristics of low density, low damage, strong sand carrying capacity, good mobile control performance, etc. [1–5]. As a common plugging agent, the foam can selectively block high-permeability layers and high water saturation layers [6, 7]. In steam injection development of heavy oil, the foam can prevent steam channeling, control steam overlay, and expand steam swept volume, which improves heat utilization efficiency and thermal development performance [8–14]. However, as a thermodynamically unstable system, its performance is influenced by temperature considerably. At high temperature, foam stability declines dramatically, and the blocking performance is badly unsatisfactory, which greatly limits the application of foam in thermal recovery.

In order to study the foam flow behavior in porous media, extensive researches have been carried out in core or sandpack experiments, in which pressure drop, saturation, and foam texture were measured, and blocking effect was analyzed [15–20]. Foam texture refers to the characteristics of the foam system, including the average diameter, uniformity, and density. Bubble morphology refers to the appearance of the individual bubble, including the size and shape. CT technology was also used to investigate transient foam flow and elucidate the mechanisms of foam mobility control [21, 22]. It was found that foam flowed through sandpack continuously breaking and reforming, and foam mobility decreased in two steps: initial forward foam propagation and secondary backward liquid desaturation. The mechanism of foam propagation seemed to be initial gas channeling, progressively becoming more uniform as foam blocked the channels. Pang [23] studied the effect of surfactant concentration, foam quality, the injection rate of liquid and gas, permeability, temperature, and oil saturation on blocking ability. Osterloh and Jante [24] studied the impact of the fractional flow of gas on steady-state foam flow. They

found that foam propagated in a piston-like manner during the transient displacement, and the regime of foam flow changed with the fractional flow of gas greatly. The geometry of porous media also has a big influence on flowing behavior of foam and foam texture [25–27].

A visualization experiment in the micromodel is also widely used to investigate the flow behavior of foam in porous media, which provides an effective method to analyze foam flow and flow mechanism [28–34]. The mechanisms of snap-off, lamella division, and dynamic capillary-pressure-induced lamella drainage in foam flow studies were observed. The foam flow phenomena were sensitive to the mode of injection, the local capillary environment, and the geometry of the pore structure. The foam flow behavior in porous media at the pore level was investigated. Gas moved through pore throats by way of modified bubble train flow with a smaller bubble size. It was easy for the bubble to be trapped in larger pores because of insufficient moving force. The lamellae were stable, and the liquid drainage resulted in breaking and reforming events. The liquid flowed through the network of films in the presence of foam, whereas gas was displaced by lamellae in long bubbles. Snap-off was the main mechanism to generate the bubble. Liquid and gas resided in pores in foam, leading to a considerable reduction in effective air mobility.

Theoretical researches were also conducted from different aspects. The effects of static and interfacial properties of foam on flow characteristic and blocking capacity were studied, between which there was a relationship to a certain extent [35–37]. Wang et al. [18] established a mathematical model of foam resistance factor under influencing factors of foaming agent concentration, foam quality, permeability, temperatures, and oil saturation based on sandpack tests. Wang et al. [38] proposed a structure evolution model based on fractal theory, in which foam structure and bubble number were analyzed emphatically. The foam texture (bubble size) in sandpack was observed by a visualization cell, in which foam texture directly corresponded to flow behavior. It was found that finer-textured foam led to larger flow resistance [39–41]. Some foam flow models have been proposed to simulate foam flow and reveal the blocking mechanism [42–46]. There was one thing in common in all models that foam texture was considered to be a determining factor for foam flow behavior. So it is necessary to analyze the foam texture to explain flow behavior.

Based on the previous studies, it can be concluded that the bubbles essentially influence foam flow behavior and blocking capacity. However, it is difficult to observe and analyze the bubble morphology in core or sandpack because of opaqueness. In order to solve this problem, a modified experimental system combining the sandpack model with the visualization micromodel was applied, in which the foam observed in the visual micromodel was approximately regarded as the same foam in sandpack [39–41]. The relationships between foam texture and flow behavior have been studied, but these studies are just qualitative and not comprehensive, with some other foam features not considered except bubble size.

In this paper, in order to further understand the foam flow behavior from the aspect of foam texture, experiments at four temperatures were conducted to observe the foam texture in the micromodel and measure the flowing pressure along the sandpack simultaneously. On this basis, a correspondence between blocking pressure and foam texture was established, and the correlation was quantitatively analyzed by correlation analysis and path analysis. In addition, the effect of temperature on foam flow behavior was analyzed from the perspective of interfacial properties.

2. Experiment

2.1. Materials. A compounded surfactant system, produced by Qingtian Natural Plant Technology Co. Ltd (Zhejiang, China), was used to generate foam. The compounded surfactant system comprises a biological surfactant (saponin of Camellia oleifera), a variety of additives (dodecyl dimethyl betaine, coconut diethanolamide, and lauryldimethylamine oxide), and deionized water. The molecular structure of saponins of Camellia oleifera is shown in Figure 1. The effective content of the surfactant system is 45 wt%, with a pH value between 7.5 and 8 and a density of 1.03-1.04 g/cm^3. At 25°C and atmosphere pressure, its interfacial tension is 22.5 mN/m when the concentration is 0.5%. The water used was distilled water. The gas used to generate foam was nitrogen with a purity of 99.9%, supplied by Tianyuan Inc. (China).

2.2. Experimental Apparatus. Figure 2 shows the schematic of the combined system used to measure the pressure and observe the foam texture. The surfactant solution was injected by the ISCO pump (Model 100DX, Teledyne Technologies). The gas injection rate was controlled by the gas mass-flow controller (Model SLA5850S, Brooks). The sandpack had a length of 60.0 cm and an inner diameter of 2.54 cm, on which four pressure transducers (Model 3210PD, the accuracy of 0.001 MPa) were equally distributed. The four positions of pressure transducers were named points 1, 2, 3, and 4 from the inlet to the outlet. Points 2, 3, and 4 were connected with the glass-etched micromodel to observe the real-time morphology of the flowing bubble. The micromodel was placed in a holder, and its size was 40 mm × 40 mm. To minimize the impact of porous media in the micromodel on bubble morphology, the pore size in the micromodel should be as similar to the sandpack model as possible. The average pore throat radius of the sandpack can be obtained approximately by

$$r = \sqrt{8k/\varnothing^{3/2}}, \quad (1)$$

where r is the average pore throat radius of the sandpack, in μm; k is the permeability of the sandpack, in μm^2; and $\varnothing$ is the porosity of the sandpack. Thus, the used micromodel with a flow channel of 10-100 μm in width and depth is satisfactory. The foam images in the micromodel were recorded by a digital camera (Model L110 Nikon). The sandpack and the micromodel were wrapped in an electric heating jacket, as shown in the figures. The pipelines linking the sandpack to the micromodel were wrapped by an electric heating belt. The temperature of the electric heating jacket and the electric heating belt were

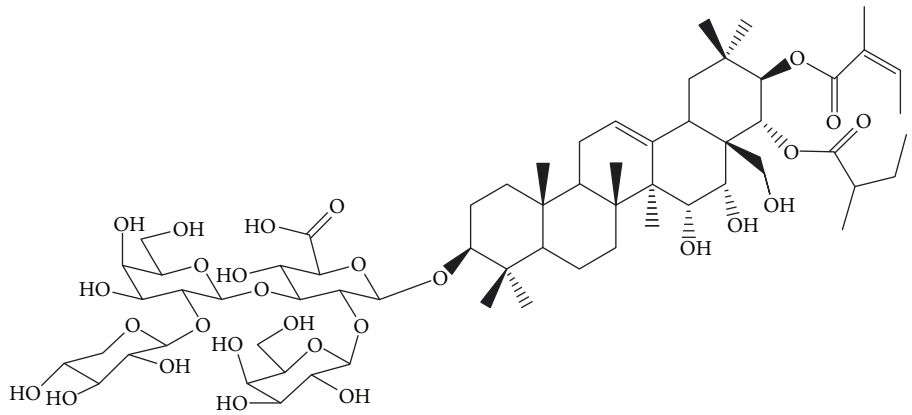

Figure 1: Molecular structure of saponins of Camellia oleifera.

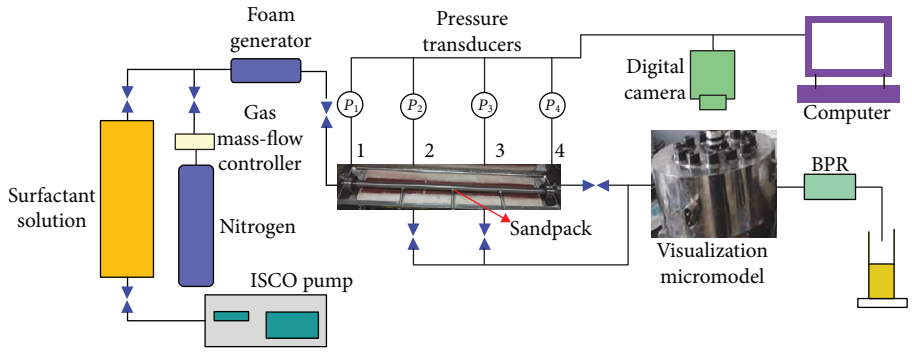

Figure 2: Flow chart of the combined experimental system of the sandpack and micromodel.

set through the temperature controller. The thermocouple with a precision on the order of 0.1°C was used to measure the temperature of the sandpack, the micromodel, and the pipelines. A backpressure regulator (BPR) with an accuracy of 0.01 MPa was used to control the pressures of the sandpack and the micromodel. The backpressure was set to 2 MPa to prevent the water from evaporation when the temperature goes above 100°C.

2.3. Experimental Procedures. The experimental procedures were as follows. (1) The core was prepared in the sandpack with silica sand, and the surfactant solution with a concentration of 1.0% was prepared. (2) The sandpack was evacuated for more than 4 hours and then saturated with distilled water with porosity and permeability calculated. (3) The apparatuses were connected, and the heating casing was set to the experimental temperature. (4) After the temperatures of the sandpack and micromodel reached stability, surfactant solution and gas were injected at the same injection rate of 1.0 mL/min under experimental conditions until displacement pressures were almost unchanged. (5) During foam flow, pressures were recorded and the foam morphologies at different positions were observed in the visualization micromodel by changing the pipeline connection with the sandpack. The detailed experimental parameters are shown in Table 1.

Table 1: Experimental parameters and conditions.

Item	Unit	Test 1	Test 2	Test 3	Test 4
Temperature	°C	20	60	100	150
Sandpack length	cm	60.0	60.0	60.0	60.0
Sandpack diameter	cm	2.54	2.54	2.54	2.54
Porosity	%	36.8	35.4	37.3	37.1
Permeability	10^{-3} μm^2	5020	4976	5045	5086
Gas-liquid ratio*	cm^3/mL	1 : 1	1 : 1	1 : 1	1 : 1
Backpressure	MPa	2.0	2.0	2.0	2.0
Total injection rate	mL/min	2	2	2	2

*The gas injection rate is under the experimental condition.

3. Image Processing and Morphological Parameter Acquisition

Cell size analysis (CSA), a FoamScan-affiliated software (Teclis, France), was used to process the microscopic image of flowing foam and obtain the morphological parameters.

3.1. Image Processing, Segmentation, and Bubble Distinguishing. To enhance adaptability and accuracy in image segmentation, a series of steps were performed on the original image, such as gray-scale transformation, image smoothing and filtering, noise reducing, binarization, and edge detection

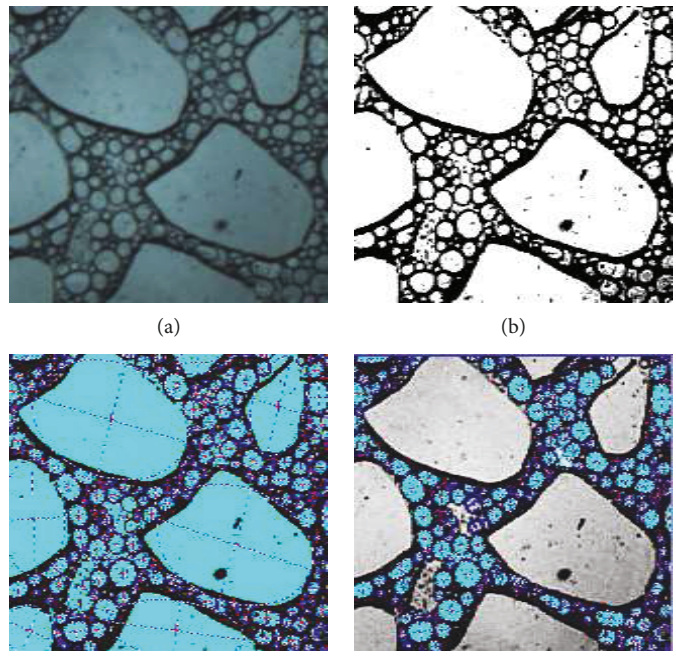

Figure 3: Foam images before and after processing. (a) is the original image observed directly. (b) is the image after binarization. (c) is the image after segmentation. (d) is the image after recognition.

and extraction. The key of image processing was threshold selection, in which a histogram arithmetic was applied. The processed image is shown in Figure 3(b), and Figure 3(a) is the original picture. It can be seen that the image is clearer and bubbles become more distinct after processing. The foam can be clearly divided into two parts, the bubble formed by gas (white color) and the lamella formed by liquid (black color). But the bubbles, the liquid between bubbles, and the solid matrix in the micromodel are indistinguishable because of the same color, as is shown in Figure 3(c). Therefore, some other methods should be considered to distinguish the bubble from the other two white parts.

In order to distinguish the bubbles, three recognition steps were conducted. First, the solid matrix could be distinguished easily according to its size, for the bubble is much smaller than the solid matrix. Next, it can be seen that the bubbles are almost round, whereas the liquid parts between bubbles are of irregular shapes. Due to the difference in shape, a criterion was proposed to distinguish the bubbles from the liquid parts that the figure with a roundness greater than 0.6 would be treated as a bubble. The roundness represents the regularity of the shape, which can be described as follows:

$$R = \frac{4\pi S}{L^2}, \tag{2}$$

where R represents the roundness of a figure, S represents the area in μm^2, and L represents the perimeter in μm. The area and perimeter of the liquid part between bubbles can be calculated by the software. The greater the roundness, the more regular the shape, and the closer it is to a circular shape.

At last, some parts that could not be distinguished from the bubbles in the first two steps could be excluded manually. Figure 3(d) shows the final result, in which the solid matrix and the liquid part between bubbles were distinguished and excluded. The comparison of Figures 3(c) and 3(d) proves that the three steps satisfy the requirement of bubble recognition.

3.2. Foam Texture Analysis. On the basis of bubble recognition, the number of bubbles could be counted and the area of each bubble could be calculated by the software. The bubble can be regarded as circular, so the equivalent diameter can be easily obtained to describe the size of a bubble. In order to describe the features of foam texture, the following three parameters were defined: average diameter, filling ratio, and variation coefficient.

The average diameter, describing the average size of bubbles, was defined as

$$\bar{d} = \frac{\sum_{i=1}^{n} d_i}{n}, \tag{3}$$

where d_i represents the equivalent diameter of the ith bubble; n represents the total number of bubbles.

The filling ratio was defined as the ratio between the total volume of bubbles and the pore volume, as shown in equation (4). The bubble and the pore in the micromodel can be regarded as two-dimensional, so the volume can be replaced by the area.

$$F = \frac{\sum_{i=1}^{n} V_i}{V_p} = \frac{\sum_{i=1}^{n} S_i}{S_p}, \tag{4}$$

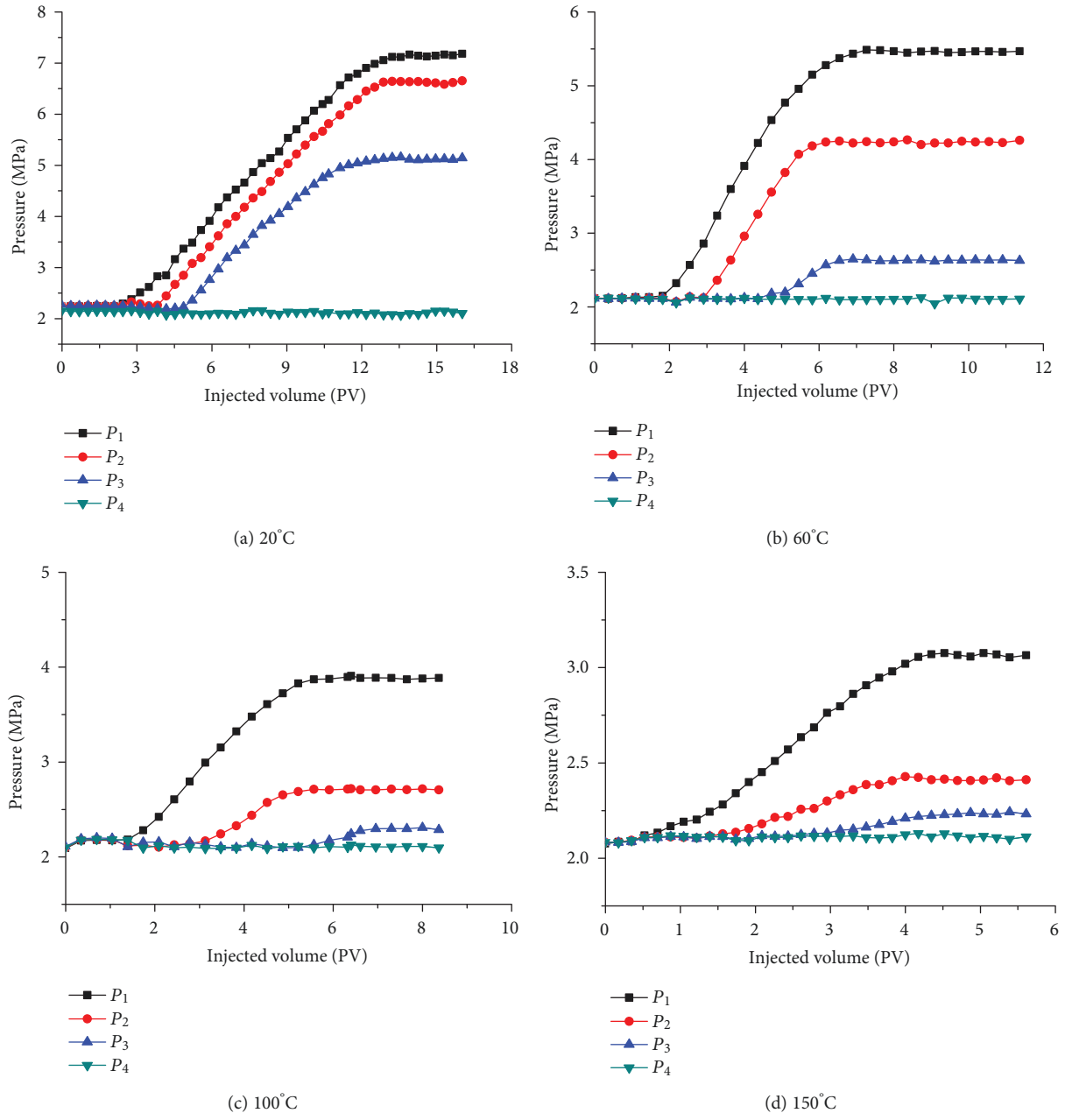

Figure 4: Change of flowing pressure with injected volume at different temperatures.

where V_i and S_i represent the volume and area of the ith bubble; V_p and S_p represent the volume and area of the pore; and n represents the total number of bubbles.

The variation coefficient, which represented the uniformity of bubble size, was defined as

$$C_v = \frac{\sqrt{1/n\sum_{i=1}^{n}\left(d_i - \bar{d}\right)^2}}{\bar{d}}, \quad (5)$$

where d_i is the equivalent diameter of the ith bubble; $\bar{d}$ is the average diameter; n represents the total number of bubbles.

4. Results and Discussion

4.1. Pressure Behaviors of Foam Flow in Sandpack. The corresponding pressures at points 1, 2, 3, and 4 were represented as P_1, P_2, P_3, and P_4. The sandpack was evenly divided into 3 sections, namely, entrance section, middle section, and export section. The changes of flowing pressure with injection volume at different temperatures are shown in Figure 4. The pressure distributions at steady state are shown in Figure 5.

In order to analyze the blocking capacity of foam, the comparisons of resistance factors on different sections are shown in Figure 6. Resistance factor is defined as the ratio

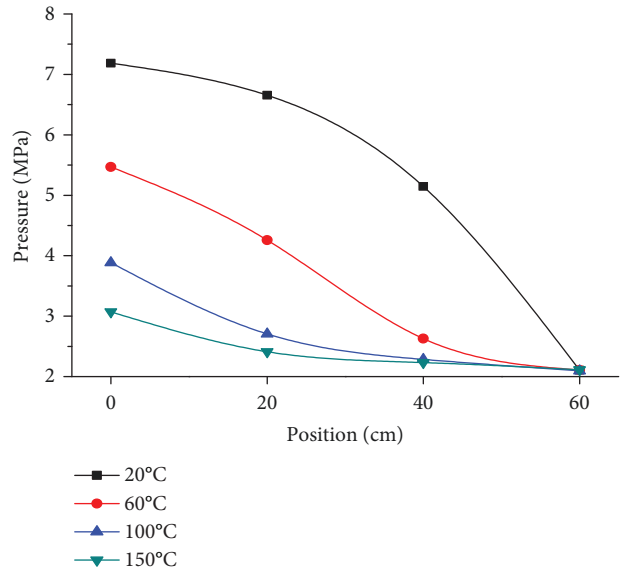

Figure 5: Pressure distribution along the sandpack under steady state at different temperatures.

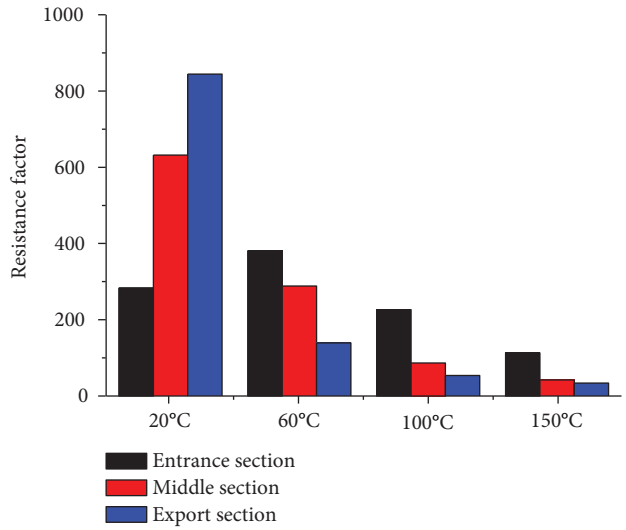

Figure 6: Comparison of the resistance factors on different sections at different temperatures.

of foam flow pressure and water flow pressure, as shown in the following equation:

$$R = \frac{\Delta P_f}{\Delta P_w}, \quad (6)$$

where R is the resistance factor; ΔP_f is the displacement pressure when foam flows; and ΔP_w is the displacement pressure when water flows.

In Figure 6, the resistance factor decreases with the increase in temperature, which indicates that the blocking capacity of foam declines. At 20°C, the resistance factor increases gradually from the entrance section to the export section, which demonstrates that the blocking capacity increases as foam flows further into the sandpack. At 60°C, the resistance factor first increases and then decreases, and the resistance factor on the export section is far less than on the first two sections. However, at 100°C and 150°C, the resistance factor decreases gradually from the entrance section to the export section, and only on the entrance section does there exist a significant resistance factor. These indicate that as the temperature increases, the blocking capacity of foam at the downstream sandpack decreases first, with the blocking scope decreasing and moving towards the inlet.

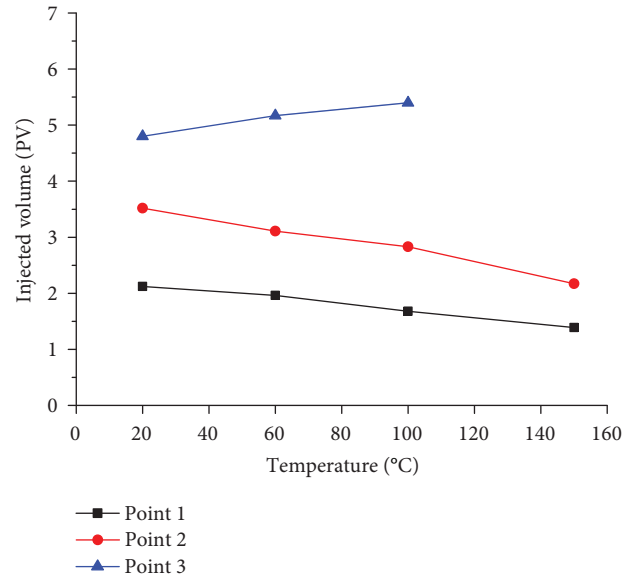

Figure 7: Change of foam arrival time with the temperature at different positions.

The time that the pressure starts to increase can be regarded as the arrival time of foam. Figure 7 compares the time that foam arrived at the different positions of the sandpack under the different temperatures.

With the increase in temperature, the foam arrival time at point 1 and point 2 decreased gradually, but the arrival time at point 3 increased. The foam arrival time at point 1 and point 2 is related to the adsorption of the surfactant on the porous media. With the increase in temperature, the adsorption capacity declines gradually. So less amount of the surfactant is required to generate the foam at a higher temperature. Under the same injection conditions, the arrival time of foam decreases with the increase in temperature. However, the arrival time at point 3 is more determined by the foam film strength. With the increase in temperature, the foam film strength declines. It is easier for foam to rupture at a higher temperature. So with the increase in temperature, more foam is required to be injected to block the porous media at point 3. As a result, the foam arrival time at point 3 increased with the temperature.

4.2. Foam Texture under Steady Flow State. After the pressures along the sandpack reached stability, microscopic images of flowing foam at points 2, 3, and 4 were observed,

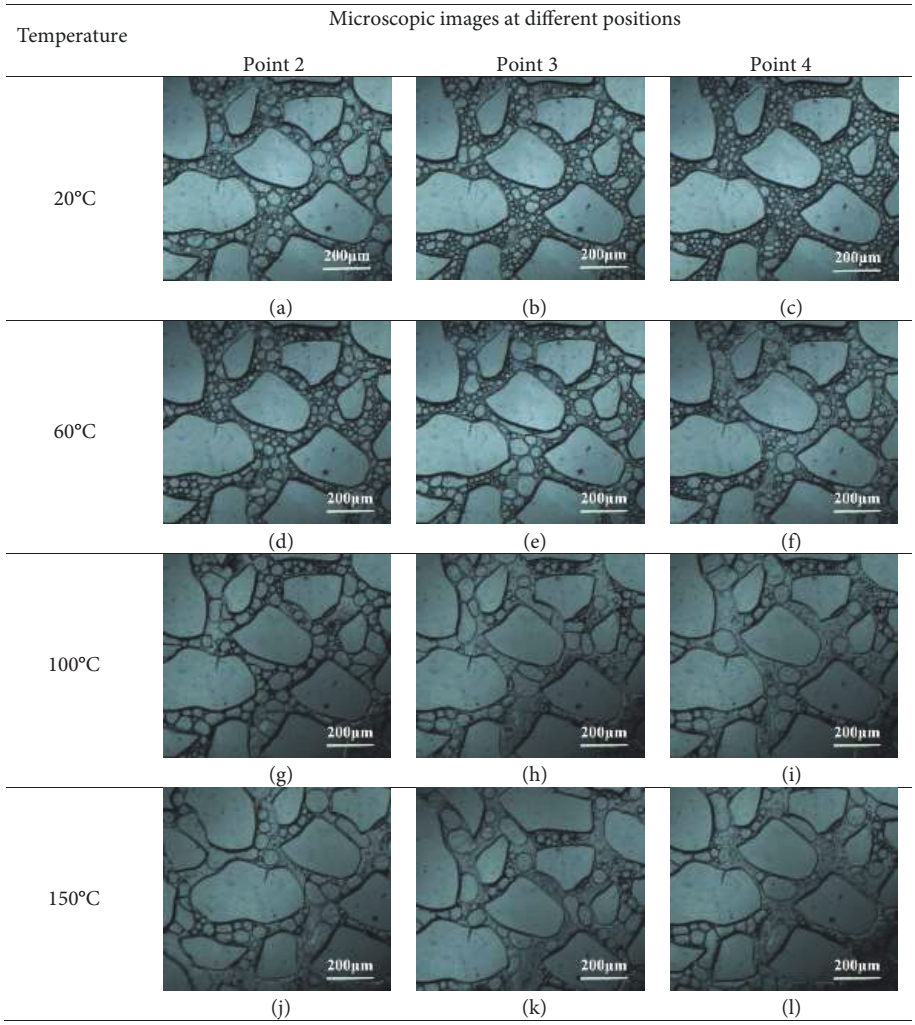

Figure 8: Foam texture observed in the micromodel at different positions and temperatures.

Table 2: Foam texture parameters and its corresponding blocking pressures.

Picture number	Average diameter (μm)	Filling ratio	Variation coefficient	Block pressure (MPa)
a	26.76	0.72	0.48	1.02
b	22.55	0.88	0.32	2.27
c	18.26	0.94	0.27	3.04
d	28.02	0.94	0.38	1.42
e	30.37	0.77	0.55	1.08
f	31.76	0.66	0.54	0.52
g	38.72	0.86	0.45	0.80
h	42.63	0.59	0.48	0.31
i	44.05	0.56	0.48	0.19
j	45.33	0.71	0.43	0.40
k	45.56	0.53	0.45	0.15
l	45.46	0.52	0.46	0.12

as is shown in Figure 8. The detailed texture parameters are shown in Table 2.

It can be seen that with the increase in temperature, the overall trend for foam texture is to have a large bubble size and scattering distribution. At 20°C, as foam flows downstream, the average diameter and the variation coefficient decrease, and the filling ratio increases, with bubbles tending to be tiny, dense, and homogenous. However, contrary to the

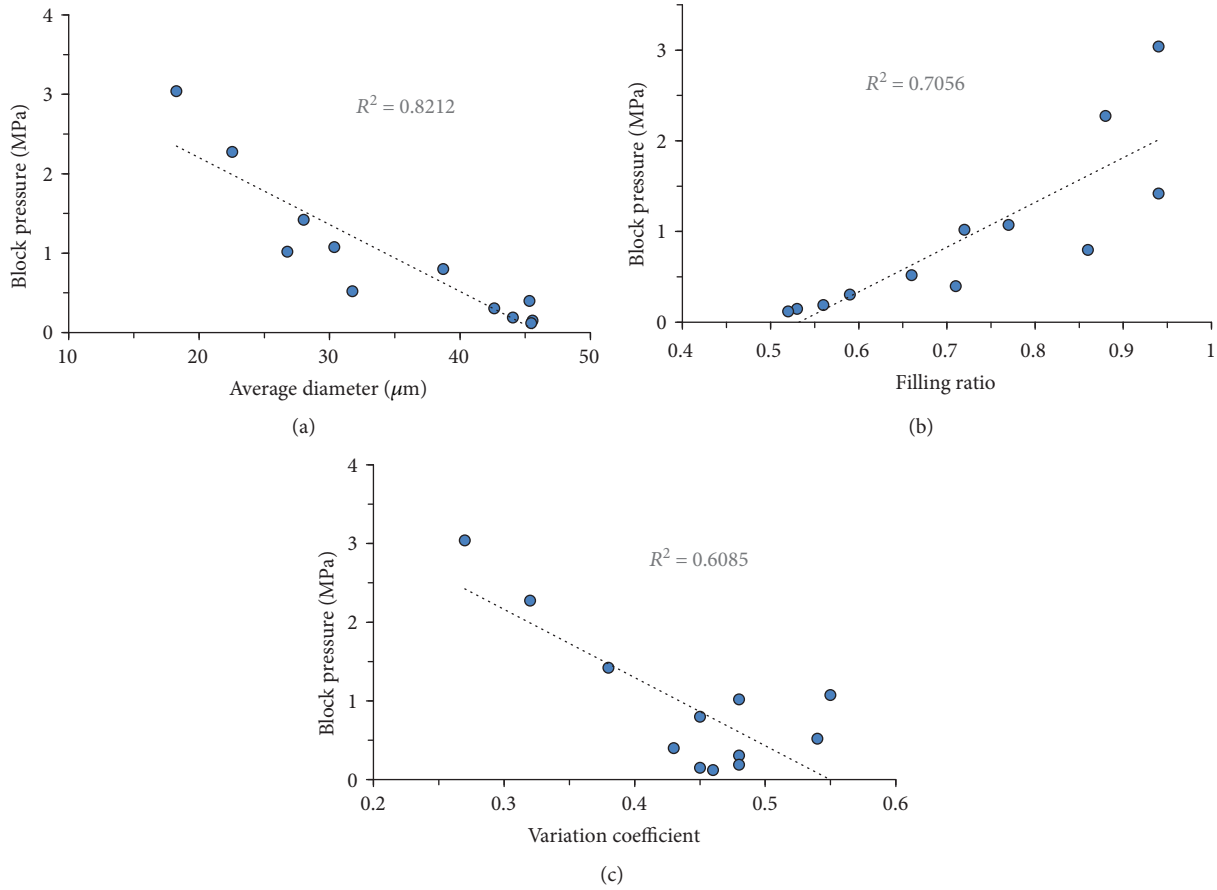

Figure 9: The relationships between foam texture and block pressure. (a) is the relationship between average diameter and block pressure. (b) is the relationship between the filling ratio and block pressure. (c) is the relationship between the variation coefficient and block pressure.

changes at 20°C, there is a tendency to become scattering and ununiform for foam texture at 60°C and 100°C. Especially at 100°C, only the entrance section is filled with dense and uniform foam. At 150°C, foam presents the characteristics of a large bubble, varying size, and straggling flow along the whole sandpack.

4.3. Correlation Analysis between Foam Texture and Pressure Behavior. It can be inferred from the results above that foam flow behavior is closely related to foam texture. Temperature influences the distribution and morphology of bubble in the sandpack, and as a result, flowing pressures behave differently. The blocking performance of foam in each picture can be approximately represented by blocking pressure, which is determined by the average value of pressure drops before and after the observation position. The corresponding blocking pressures of each foam image are shown in Table 2. Therefore, it is of great significance to establish and analyze the corresponding relationship between texture parameters and block pressure for fully understanding the blocking mechanism of foam.

The relationship between blocking pressure and average diameter, filling ratio, and variation coefficient are displayed in Figure 9, respectively. The linear relationship between average diameter and block pressure has the biggest R-squared ($R^2 = 0.8212$). The R-squared of the linear relationship between filling ratio and block pressure is 0.7056. The R-squared of the linear relationship between variation coefficient and block pressure is 0.6058. The closer to 1 the R-squared is, the more reliable the linear relationship. These show that the three parameters have linear relationships with blocking pressure to a certain extent, but more relationships need to be analyzed. So the correlation analysis and path analysis were carried out.

4.3.1. Correlation Analysis. Pearson correlation coefficients among blocking pressure and foam texture parameters have been calculated and are shown in Table 3. The blocking pressure presents a negative and strong correlation with the average diameter ($r = -0.906$) and variation coefficient ($r = -0.78$), but exhibits a positive correlation with the filling ratio ($r = 0.84$), all of which have a very good significance threshold ($P < 0.01$).

Among foam texture parameters, the filling ratio negatively correlated well with the average diameter and variation coefficient ($P < 0.05$). But there is no significant correlation between average diameter and variation coefficient ($P > 0.05$).

Because of the interactions among variables, the Pearson correlation coefficient cannot really show the correlation. Accordingly, the partial correlation analysis is conducted to analyze the real correlation between the blocking pressure and the texture parameters in Table 4. With the effect of

Table 3: Pearson correlation matrix.

Pearson correlations	Average diameter	Filling ratio	Variation coefficient	Block pressure
Average diameter				
Coefficient	1			
Sig. (2-tailed)	0.000			
Filling ratio				
Coefficient	-0.793**	1		
Sig. (2-tailed)	0.002	0.000		
Variation coefficient				
Coefficient	0.506	-0.613*	1	
Sig. (2-tailed)	0.093	0.034	0.000	
Block pressure				
Coefficient	-0.906**	0.840**	-0.780**	1
Sig. (2-tailed)	0.000	0.001	0.003	0.000

**Correlation is significant at the 0.01 level (2-tailed). *Correlation is significant at the 0.05 level (2-tailed).

Table 4: Partial correlation between block pressure and texture parameters.

Control variables	Partial correlation		Block pressure
Filling ratio & variation coefficient	Average diameter	Coefficient	-0.892**
		Sig. (2-tailed)	0.001
Variation coefficient & average diameter	Filling ratio	Coefficient	0.271
		Sig. (2-tailed)	0.449
Average diameter & filling ratio	Variation coefficient	Coefficient	-0.856**
		Sig. (2-tailed)	0.002

**Correlation is significant at the 0.01 level (2-tailed).

variables excluded, the blocking pressure still has significant negative correlations with the average diameter and variation coefficient ($P < 0.01$). However, the blocking pressure presents a low positive correlation with the filling ratio, and this correlation has no statistical significance ($P > 0.05$). These suggest that the locking capacity of foam is really related to the average diameter and variation coefficient.

4.3.2. Path Analysis. The correlation analysis simply gives the correlation between variables, but may not provide a clear understanding of how texture parameters affect block pressure. Path analysis offers a method of recognizing the effects and measuring the relative importance of the causal factors. In this study, the Pearson correlation coefficients were divided into the direct effect of texture parameters on block pressure and the indirect effects caused by the interrelation among texture parameters. The results of path analysis are shown in Table 5.

The average diameter shows the highest negative direct effect on blocking pressure (-0.624) and small indirect effect via the filling ratio (-0.077) and variation coefficient (-0.205). The filling ratio shows a pretty small positive direct effect (0.097), whereas its indirect effects via average diameter (0.495) and variation coefficient (0.248) are relatively great. The variation coefficient has a negative direct effect (-0.404) and negative indirect effect via the average diameter (-0.316) and filling ratio (-0.060). Not only do the average diameter and variation coefficient have a great direct effect on blocking pressure, but also the indirect effects via them are significant. However, for the filling ratio, the direct effect and the indirect effect via it are both very small, which means that the influence of the filling ratio on blocking pressure is mainly exerted by the interaction with other factors. These also indicate that the average diameter and variation coefficient are the factors that really influence blocking pressure.

4.4. Effect of Interfacial Properties of Foam on Flow Behavior. The changes of foam flow behavior with temperature can be explained by the interfacial properties of the bubble film [47–51]. The generation of foam is a process that the surface area and the energy of system increase. The decrease of the interfacial tension can decrease the surface energy of the foam system. In general, the lower the interfacial tension, the better the foaming capacity. Because of the adsorption of the surfactant on the gas-liquid interface, the bubble film is a viscoelastic film. The viscoelasticity of the bubble film can be characterized by the interfacial parameter–viscoelastic modulus, which consists of two parts: elastic modulus and viscous modulus. The elastic modulus shows the restorability of the bubble film after deformation, and the viscous modulus shows the strength of the bubble film and the capacity to resist the disturbance. When foam flows in porous media, the intense shear action makes the bubbles to deform, collapse, and regenerate continually. The foam texture in the

Table 5: The direct and indirect effects of texture parameters on block pressure.

Texture parameters	Total effect	Direct effect	Indirect effect via average diameter	Indirect effect via filling ratio	Indirect effect via variation coefficient
Average diameter	-0.906	-0.624	—	-0.077	-0.205
Filling ratio	0.840	0.097	0.495	—	0.248
Variation coefficient	-0.780	-0.404	-0.316	-0.060	—

flow process is the result of breakage and regeneration of the bubbles. The breakage of the bubble is related to the viscoelastic modulus of the film, and the regeneration of the bubble is related to the interfacial tension. So the interfacial properties are essential to foam flow behavior.

With the increase in temperature, the interfacial tension increases and the viscoelastic modulus decreases in general. Because as the temperature increases, the amount of surfactant on the interface declines, the hydration of the surfactant weakens and the evaporation of the film intensifies. At 20°C, the interfacial tension is lower and the viscoelastic modulus is higher. The film has a good elasticity and high strength. It is not easy for the bubble to break. Even if the foam bursts, it can regenerate soon due to the lower interfacial tension. The regeneration rate is greater than the breakage rate. Besides, low interfacial tension means low surface energy, which guarantees that the bubbles can stabilize in small size. So with the increase in flow distance, the foam texture tends to become tiny, dense, and uniform. At 100°C and 150°C, the interfacial tension is higher and the viscoelastic modulus is lower. In the flow process, the bubble breaks easily and cannot regenerate. So the foam texture becomes scattered and ununiform with the increase in flow distance. Only in the entrance section does the foam show the blocking performance.

5. Conclusions

In this paper, flowing pressures along sandpack were measured and foam images were observed simultaneously. On this basis, the relationship between blocking performance and foam texture was analyzed by correlation analysis and path analysis.

(1) With the increase in flow distance in a 60 cm-long sandpack at 20°C, the blocking capacity of foam increases, and the foam texture tends to become tiny, dense, and homogenous

(2) As the temperature increases, the blocking capacity of foam declines with the blocking scope decreasing and moving towards the inlet, and it is increasingly easy to become scattered and ununiform in texture

(3) The blocking pressure has a strong correlation with average diameter (-0.906) and variation coefficient (-0.78), and the direct effect of the average diameter and variation coefficient is -0.624 and -0.404. Although the filling ratio has a positive correlation with blocking pressure (0.84), the direct effect (0.097) is very small

(4) Foam flow behavior is determined by the foam texture essentially. The blocking capacity of foam is mainly influenced negatively by the average diameter and variation coefficient, suggesting that tiny, dense, and homogeneous foam has a stronger blocking capacity

Data Availability

The data used to support the findings of this study are included within the article.

Conflicts of Interest

The authors declare no competing interests.

Acknowledgments

Financial support is received by the National Natural Science Foundation of China (Grant 51604292), the Natural Science Foundation of Shandong Province, China (Grant ZR2016 EEB29), the National Science and Technology Major Project of China (Grant 2016ZX05012-002-004), the Fundamental Research Funds for the Central Universities (Grant 17CX0 2014A), the National Science and Technology Major Project of China (Grant 2016ZX05031-002-004-002), the Postdoctoral Researcher Applied Research Project Funding of Qingdao, China (040000639), and the China Postdoctoral Science Foundation (2018M632637).

References

[1] J. Wang, L. Han, S. Li, and T. Wang, "Application status and prospect of foam fluid in oil field," *Applied Chemical Industry*, vol. 41, no. 8, pp. 1408–1411, 2012.

[2] S. A. Farzaneh and M. Sohrabi, "A review of the status of foam application in enhanced oil recovery," in *EAGE Annual Conference & Exhibition Incorporating SPE Europec, Society of Petroleum Engineers*, London, UK, June 2013.

[3] Z. Li, R. Li, W. Liu, and Q. Gao, "Application and outlook of foam in oil and gas field development (II)—application of foam fluid in immediate vicinity of wellbore and formation," *Oilfield Chemistry*, vol. 30, no. 1, pp. 155–160, 2013.

[4] R. F. Li, W. Yan, S. Liu, G. Hirasaki, and C. A. Miller, "Foam mobility control for surfactant enhanced oil recovery," *SPE Journal*, vol. 15, no. 4, pp. 928–942, 2010.

[5] J. Zhang, X. Wu, Z. Chen et al., "Application and experimental study of cyclic foam stimulation," *RSC Advances*, vol. 5, no. 93, pp. 76435–76441, 2015.

[6] A. Gandomkar, R. Kharrat, M. Motealleh, H. H. Khanamiri, M. Nematzadeh, and M. H. Ghazanfari, "An experimental

investigation of foam for gas mobility control in a low-temperature fractured carbonate reservoir," *Petroleum Science and Technology*, vol. 30, no. 10, pp. 976–985, 2012.

[7] Z. Wu, H. Liu, Z. Pang, C. Wu, and M. Gao, "Pore-scale experiment on blocking characteristics and EOR mechanisms of nitrogen foam for heavy oil: a 2D visualized study," *Energy & Fuels*, vol. 30, no. 11, pp. 9106–9113, 2016.

[8] X. Lyu, H. Liu, Z. Pang, and Z. Sun, "Visualized study of thermochemistry assisted steam flooding to improve oil recovery in heavy oil reservoir with glass micromodels," *Fuel*, vol. 218, pp. 118–126, 2018.

[9] B. Mukherjee, P. D. Patil, M. Gao, W. Miao, S. Potisek, and P. Rozowski, "Laboratory evaluation of novel surfactant for foam assisted steam EOR method to improve conformance control for field applications," in *SPE Improved Oil Recovery Conference. Society of Petroleum Engineers*, Tulsa, OK, USA, April 2018.

[10] A. Suhag, R. Ranjith, K. Balaji et al., "Optimization of steam-flooding heavy oil reservoirs," in *SPE Western Regional Meeting. Society of Petroleum Engineers*, Bakersfield, CA, USA, April 2017.

[11] E. Delamaide, A. Cuenca, and M. Chabert, "State of the art review of the steam foam process," in *SPE Latin America and Caribbean Heavy and Extra Heavy Oil Conference. Society of Petroleum Engineers*, Lima, Peru, October 2016.

[12] P. Liu, W. Li, and D. Shen, "Experimental study and pilot test of urea- and urea-and-foam-assisted steam flooding in heavy oil reservoirs," *Journal of Petroleum Science and Engineering*, vol. 135, pp. 291–298, 2015.

[13] C. Lu, H. Liu, and Z. Pang, "Characteristics analysis of cold foam and hot foam during steam flooding in heavy oil reservoirs," *Petroleum Science and Technology*, vol. 32, no. 19, pp. 2321–2328, 2014.

[14] Z. Pang, H. Liu, and L. Zhu, "A laboratory study of enhancing heavy oil recovery with steam flooding by adding nitrogen foams," *Journal of Petroleum Science and Engineering*, vol. 128, pp. 184–193, 2015.

[15] B. Li, H. Li, A. Cao, and F. Wang, "Effect of surfactant concentration on foam texture and flow characteristics in porous media," *Colloids and Surfaces A: Physicochemical and Engineering Aspects*, vol. 560, pp. 189–197, 2019.

[16] A. R. Adebayo and M. Y. Kanj, "Exploring a mechanistic approach for characterizing transient and steady state foam flow in porous media," *Journal of Natural Gas Science and Engineering*, vol. 60, pp. 214–227, 2018.

[17] J. Kim, Y. Dong, and W. R. Rossen, "Steady-state flow behavior of CO2 foam," *SPE Journal*, vol. 10, no. 4, pp. 405–415, 2005.

[18] J. Wang, H. Liu, Z. Ning, and H. Zhang, "Experimental research and quantitative characterization of nitrogen foam blocking characteristics," *Energy & Fuels*, vol. 26, no. 8, pp. 5152–5163, 2012.

[19] X. Wang, J. Chen, C. Lv, and M. Wei, "Experimental investigation and evaluation on influence of foam flow resistance in porous media," *Environment and Earth Science*, vol. 74, no. 7, pp. 5729–5738, 2015.

[20] R. Thorat and H. Bruining, "Determination of the most significant variables affecting the steady state pressure drop in selected foam flow experiments," *Journal of Petroleum Science and Engineering*, vol. 141, pp. 144–156, 2016.

[21] M. Simjoo, Y. Dong, A. Andrianov, M. Talanana, and P. L. J. Zitha, "Ct scan study of immiscible foam flow in porous media for enhancing oil recovery," *Industrial and Engineering Chemistry Research*, vol. 52, no. 18, pp. 6221–6233, 2013.

[22] M. Simjoo, Y. Dong, A. Andrianov, M. Talanana, and P. L. J. Zitha, "Novel insight into foam mobility control," *SPE Journal*, vol. 18, no. 03, pp. 416–427, 2013.

[23] Z. X. Pang, "The blocking ability and flowing characteristics of steady foams in porous media," *Transport in Porous Media*, vol. 85, no. 1, pp. 299–316, 2010.

[24] W. T. Osterloh and M. J. Jante, "Effects of gas and liquid velocity on steady-state foam flow at high temperature," in *SPE/-DOE Enhanced Oil Recovery Symposium, Society of Petroleum Engineers*, Tulsa, OK, USA, April 1992.

[25] B. Géraud, S. A. Jones, I. Cantat, B. Dollet, and Y. Méheust, "The flow of a foam in a two-dimensional porous medium," *Water Resources Research*, vol. 52, no. 2, pp. 773–790, 2016.

[26] K. Osei-Bonsu, P. Grassia, and N. Shokri, "Effects of pore geometry on flowing foam dynamics in 3D-printed porous media," *Transport in Porous Media*, vol. 124, no. 3, pp. 903–917, 2018.

[27] M. Chen, Y. C. Yortsos, and W. R. Rossen, "Insights on foam generation in porous media from pore-network studies," *Colloids and Surfaces, A: Physicochemical and Engineering Aspects*, vol. 256, no. 2-3, pp. 181–189, 2005.

[28] M. A. Fernø, J. Gauteplass, M. Pancharoen et al., "Experimental study of foam generation, sweep efficiency, and flow in a fracture network," *SPE Journal*, vol. 21, no. 4, pp. 1140–1150, 2016.

[29] J. Gauteplass, K. Chaudhary, A. R. Kovscek, and M. A. Fernø, "Pore-level foam generation and flow for mobility control in fractured systems," *Colloids and Surfaces, A: Physicochemical and Engineering Aspects*, vol. 468, no. 184-192, pp. 184–192, 2015.

[30] M. M. Almajid and A. R. Kovscek, "Pore-level mechanics of foam generation and coalescence in the presence of oil," *Advances in Colloid and Interface Science*, vol. 233, pp. 65–82, 2016.

[31] K. Xu, T. Liang, P. Zhu et al., "A 2.5-D glass micromodel for investigation of multi-phase flow in porous media," *Lab on a Chip*, vol. 17, no. 4, pp. 640–646, 2017.

[32] Y. Wu, S. Fang, C. Dai et al., "Investigation on bubble snap-off in 3-D pore-throat micro-structures," *Journal of Industrial and Engineering Chemistry*, vol. 54, pp. 69–74, 2017.

[33] B. I. AlQuaimi and W. R. Rossen, "Study of foam generation and propagation in fully characterized physical-model fracture," *Journal of Petroleum Science and Engineering*, 2018.

[34] A. Anazadehsayed, N. Rezaee, J. Naser, and A. V. Nguyen, "A review of aqueous foam in microscale," *Advances in Colloid and Interface Science*, vol. 256, pp. 203–229, 2018.

[35] N. H. Nasr, S. M. Mahmood, and H. Hematpur, "A rigorous approach to analyze bulk and coreflood foam screening tests," *Journal of Petroleum Exploration and Production Technologies*, pp. 1–14, 2018.

[36] K. Osei-Bonsu, P. Grassia, and N. Shokri, "Relationship between bulk foam stability, surfactant formulation and oil displacement efficiency in porous media," *Fuel*, vol. 203, pp. 403–410, 2017.

[37] Z. Z. Wang, L. I. Zhao-Min, and L. I. Song-Yan, "Investigation of relationship between foam blocking performance and interfacial property," *Journal of Chemical Engineering of Chinese Universities*, vol. 30, pp. 216–222, 2016.

[38] F. Wang, Z. Li, H. Chen, and X. Zhang, "Establishment and application of a structure evolution model for aqueous foam based on fractal theory," *RSC Advances*, vol. 7, no. 7, pp. 3650–3659, 2017.

[39] R. A. Ettinger and C. J. Radke, "Influence of texture on steady foam flow in Berea sandstone," *SPE Reservoir Engineering*, vol. 7, no. 1, pp. 83–90, 1992.

[40] A. R. Kovscek, Q. Chen, and M. Gerritsen, "Modeling foam displacement with the local-equilibrium approximation: theory and experimental verification," *SPE Journal*, vol. 15, no. 1, pp. 171–183, 2010.

[41] J. Hou, Q. Du, Z. Li, G. Pan, X. Lu, and K. Zhou, "Experiments on foam texture under high pressure in porous media," *Flow Measurement and Instrumentation*, vol. 33, pp. 68–76, 2013.

[42] S. I. Kam, "Improved mechanistic foam simulation with foam catastrophe theory," *Colloids and Surfaces A: Physicochemical and Engineering Aspects*, vol. 318, no. 1-3, pp. 62–77, 2008.

[43] F. Wang, Z. Li, H. Chen, Q. Lv, W. Silagi, and Z. Chen, "Fractal characterization of dynamic structure of foam transport in porous media," *Journal of Molecular Liquids*, vol. 241, pp. 675–683, 2017.

[44] R. Farajzadeh, M. Lotfollahi, A. A. Eftekhari, W. R. Rossen, and G. J. H. Hirasaki, "Effect of permeability on implicit-texture foam model parameters and the limiting capillary pressure," *Energy & Fuels*, vol. 29, no. 5, pp. 3011–3018, 2015.

[45] K. Ma, G. Ren, K. Mateen, D. Morel, and P. Cordelier, "Modeling techniques for foam flow in porous media," *SPE Journal*, vol. 20, no. 03, pp. 453–470, 2015.

[46] M. Lotfollahi, R. Farajzadeh, M. Delshad, A. Varavei, and W. R. Rossen, "Comparison of implicit-texture and population-balance foam models," *Journal of Natural Gas Science and Engineering*, vol. 31, pp. 184–197, 2016.

[47] H. Zhong, W. Zhang, H. Yin, and H. Liu, "Study on mechanism of viscoelastic polymer transient flow in porous media," *Geofluids*, vol. 2017, Article ID 8763951, 8 pages, 2017.

[48] A. Andersen, J. Oertegren, P. Koelsch, D. Wantke, and H. Motschmann, "Oscillating bubble SHG on surface elastic and surface viscoelastic systems: new insights in the dynamics of adsorption layers," *The Journal of Physical Chemistry B*, vol. 110, no. 37, pp. 18466–18472, 2006.

[49] Y. Zhang, Z. Chang, W. Luo, S. Gu, W. Li, and J. An, "Effect of starch particles on foam stability and dilational viscoelasticity of aqueous-foam," *Chinese Journal of Chemical Engineering*, vol. 23, no. 1, pp. 276–280, 2015.

[50] R. Rafati, A. S. Haddad, and H. Hamidi, "Experimental study on stability and rheological properties of aqueous foam in the presence of reservoir natural solid particles," *Colloids and Surfaces, A: Physicochemical and Engineering Aspects*, vol. 509, no. 19-31, pp. 19–31, 2016.

[51] Y. Wang and J. Ge, "Effect of surface dilatational modulus on bubble generation in visualized pore-throat models," *Journal of Surfactants and Detergents*, vol. 21, no. 2, pp. 283–291, 2018.